The SPL-based Neutrino Super Beam (PRSTAB contribution)

C. Bobeth[b], O. Caretta[d], P. Cupial[a], T. Davenne[d], C. Densham[d], M. Dracos[b], M. Fitton[d], B. Lepers[b], A. Longhin[c], P. Loveridge[d], F. Osswald[b], M. Rooney[d], N. Vassilopoulos[b], A. Wroblewski[a], M. Zito[c]

[a]Cracow University of Technology, Cracow, Poland
[b]IPHC, Université de Strasbourg, CNRS/IN2P3, F-67037 Strasbourg, France
[c]Irfu, CEA-Saclay, 91191 Gif-sur-Yvette, France
[d]STFC Rutherford Appleton Laboratory, Didcot, UK

Abstract

The EUROnu Super Beam work package has studied a neutrino beam based on SPL and aimed at MEMPHYS, a large water Cherenkov detector, proposed for the Laboratoire Souterrain de Modane (Fréjus tunnel, France), with a baseline of 130 km. The aim of this proposed experiment is to study the CP violation in the neutrino sector.

In the study reported here, we have developed the conceptual design of the neutrino beam, especially the target and the magnetic focusing device. Indeed, this beam present several unprecedented challenges, like the high primary proton beam power (4 MW), the high repetition rate and the low energy of the protons. The design is completed by a study of all the main component of the system, starting from the trasport system to guide the beam to the target up to the beam dump.

Keywords: Super Beam, EUROnu, SPL, neutrino oscillations, target, horn

Contents

2

1. Introduction

The EUROnu Super Beam work package has studied the project of a neutrino beam based on SPL and aimed at MEMPHYS, a large water Cherenkov detector, proposed for the Laboratoire Souterrain de Modane (Frejus, France), with a baseline of 130 km. The aim of this proposed experiment is to study the CP violation in the neutrino sector.

In the study reported here, we have developed the conceptual design of the neutrino beam, especially the target and the magnetic focusing device. Indeed, this beam present several unprecedented challenges, like the high primary proton beam power (4 MW), the high repetition rate and the low energy of the protons. The design is completed by a study of all the main component of the system, starting from the trasport system to guide the beam to the target up to the beam dump.

The report is organized in the following way. In this section, we briefly present the overall system, with references to the previous studies and a summary of the main parameters and dimensions. We then present the various components, the beam switch yard (section 2), the target station (Section 3), the target (section 4), the horn (section 5) . Finally, the study of the activation and shielding of the system is presented in section 6 and the optimization tool, neutrino fluxes and physics performances in section 7. This report presents only a summary of the main results obtained in the course of this study. A more complete description can be found in [1] as well as in the various reports [2].

First studies of this facility [3, 4, 5] were performed assuming a 2.2 GeV proton beam and a liquid mercury jet target associated with a single conic horn with a pulsed current of 300 kA. Later it was proposed [6] to supplement the system with an auxiliary horn (called reflector) enclosing concentrically the first horn and operated at 600 kA in order to focus also pions produced at larger angles. This scheme was adopted in [7] and the horn shape re-optimized using the method described in [8]. Further, the decay tunnel was re-optimized using different primary beam energies from 2.2 up to 8 GeV. Based on the neutrino fluxes of [7] and an improved parametrization of the far detector, the physics performances of the project were presented in [9] assuming a 3.5 GeV proton kinetic energy.

With respect to previous studies on this subject we propose a new design based on the use of a solid target and a single magnetic horn operated with a lower value of the pulsed current (300-350 kA). Such a setup simplifies the engineering complexity of the system avoiding difficult issues such as the containment of the mercury jet in a magnetic field free region, the challenge of a power supply operating

4

at 600 kA and the constraints related to mechanical stresses on the horn-reflector system induced by the high frequency current pulsing.

The proton beam for this facility will be provided by the high power SPL, followed by an accumulator ring. To reduce the challenge on the target and the horn system, in particular the heat to be removed, the stresses and the radiation damage, we have forseen a set of four identical target and horn units. Each target will then receive a full beam spill every 12.5 s for a total power of 1 MW.

We present a view of the beam transport and distribution system in Fig. 1. The beam line, with a total length 30 m, is composed of two kickers, and then one dipole and three quadrupoles on each of the four separate transport lines.

The target station is shown in Fig. 2 and consists of the four targets and horns within a single large helium vessel. It is followed by the decay volume with a length of 25 m and by the beam dump. The thickness of the shielding around the decay volume is 2.2 m iron and 3.7 m concrete.

The target (78 cm long and 2.4 cm diameter) is a made out of a titanium can filled with 3 mm diametertitanium spheres. It is cooled by a transversal helium flow.

Each target is inserted inside a 2.5 m long magnetic horn, pulsed with a current of 300 kA.
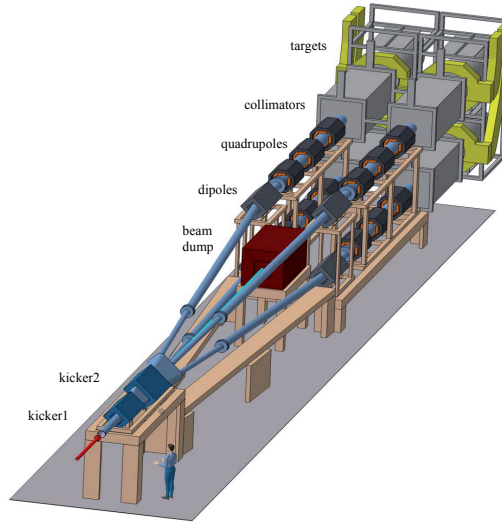

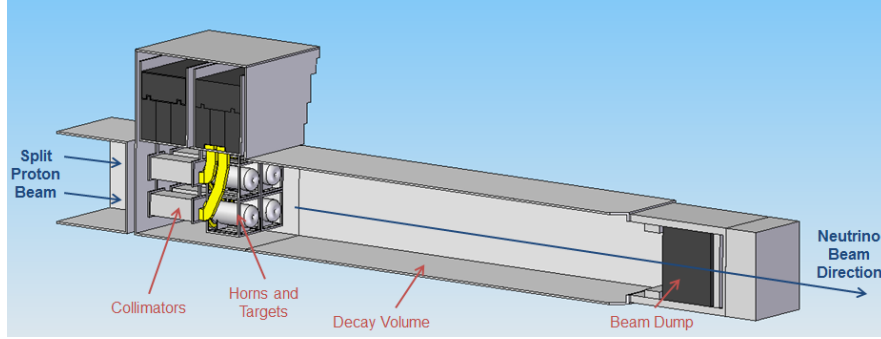Figure 1: The beam transport and distribution system.

Figure 2: Components of Target Station Beamline

2. The beam transport and distribution

2.1. The superconducting proton linac (SPL)

The proton driver foreseen for the SPL-Super Beam is the High Power Super Conducting Proton Linac (HP-SPL) under study at CERN. The current design studies [11, 12] consider a beam power of 4 MW at 50 Hz repetition frequency with protons of about 4.5 GeV kinetic energy and a pulse duration of about 600 μs for neutrino physics applications. The parameters considered for the SPL in the latest study are reported in Table 1.

2.2. The accumulator ring

The pulse duration of the proton beam delivered on the SPL-Super Beam target-horn station should be less than $5~\mu$s [15, 16] . For this reason an additional accumulator ring is required interfacing the SPL and the target-horn station.

Dedicated design studies have been performed for the Neutrino Factory [13, 17] which requires a combination of accumulator and compressor rings in order to achieve a bunch length of 2 ns rms after compression. For the Super Beam the accumulator ring is sufficient and among the considered scenarios the 6-bunch per pulse option is most suited allowing for the lowest values of the local power distribution inside the target. This scenario foresees 6 bunches per pulse with bunch length 120 ns and gaps of 60 ns. The longitudinal bunch profile has a trapezoidal shape with the linear density rising and falling linearly at the beginning and end within 10 ns in order to avoid longitudinal instabilities.

Parameters	Value
Energy	4.5 GeV
Beam power	4.0 MW
Rep. rate	50 Hz
Average pulse current	40 mA
Transverse emittances	3π.mm.mrad
Sigma	2 mm
Peak pulse current	64 mA
Chopping ratio	62 %
Beam pulse length	0.6 ms
Protons per pulse for PS2	1.5×10^{14}
Beam duty cycle	2.0 %
Number of klystrons (LEP)	14
Number of klystrons (704 MHz)	57
Peak RF power	219 MW
Average power consumption	38.5 MW
Cryogenics av. Power consumption	4.5 MW
Cryogenic temperature	2.0 K
Length	534 m

Table 1: Parameters of the HP-SPL[13, 14]

2.3. Beam distribution onto the horn system

The incoming proton beam from the accumulator needs to be splitted into 4 different beams and impinges on the 4-target-horn system at a frequency of 12.5 Hz. The general conceptual layout of the beam distribution is presented in Figure 3.

The four targets are separated by a distance of 2000 mm (centre-to-centre). This value is a key parameter in the design of the beam distribution system as it determines the angle of deflection and thus the magnetic field mandatory for the splitting of the proton beam. The requirement on the Gaussian width of the beam is 4 mm. The primary proton beam coming from the accumulator is assumed to propagate along the z axis centred onto the 4-targets-horn system; two angles of deflection are therefore needed to bring the protons to the axis of each target. The use of two bipolar kickers would then be suitable to perform this task.

The two bipolar kickers make an angle of 45 degrees with respect to the central

Parameters	Value
Energy	4.5 GeV
Relativistic γ	6.32907
Number of bunches	6
Beam size, σ	2 mm
Transverse emittances (rms)	3π.mm.mrad
Total bunch length	120 ns
RMS momentum spread (dp/p)	0.863×10^{-3}
Circumference	318.448 m
Average β function (β_x, β_y)	20,20 m
Momentum compaction, α_0	0.0249643
Nominal tune, Q_x/Q_y	7.77, 7.77
Natural chromaticity, Q'$_{nat}$	-8.4, -7.9
2nd order momentum compaction, α_1	4.68
Beam pipe half-height	50 mm

Table 2: Parameters of the accumulator[17, 19]

beam axis. This rotation already introduces a first angle of deflection. Therefore, according to the polarity of the magnetic field of K1 (K2), the proton beam is distributed diagonally to the compensating dipoles D1 or D3 (D2 or D4) which deviate the beam to the corresponding target T1 or T3 (T2 or T4). To avoid unwanted optical phenomena as achromaticity and to have the beam hitting the target with an incident angle of 90 degrees the optical system has to be symmetrical. Therefore compensating dipoles (D1, D2, D3 and D4) are needed.

A diagram of the operation mode of each optical element involved in this configuration can be therefore suggested. A few ms before the protons enter the
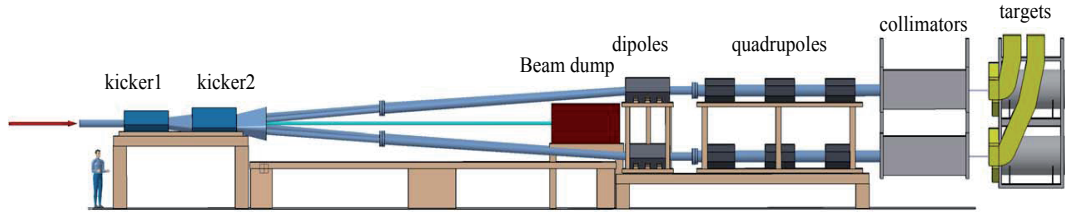

Figure 3: Side view of the distribution system.

8

kicker system, the magnetic field of one of the two kickers increases to reach its maximum value. When getting between the magnets of the kicker, the protons are subject to the magnetic force induced and then are deflected by the angle $\pm\ \alpha$ to the corresponding compensating dipole. The repetition rate for the whole horn system is 20 ms (50 Hz) which gives a rate of 80 ms (12.5 Hz) for each of the targets. Having 2 kickers in series implies the use of a consequent aperture of the second kicker in order to prevent the beam kicked from the first kicker to hit the magnet of the second one.

At a distance of 15 m and at a proton energy of 4.5 GeV, the kickers must induce a magnetic field of 0.86 T to deflect the beam to the axis of the compensating dipoles. The vertical aperture of the second kicker (K2) should be at least 60 cm to allow the beam to pass through without damaging the magnets. The code TRANSPORT [21] was used to estimate the size of the beam envelope between the kicker and the compensating dipole travelling through the 4 beam lines. The aim of the four beam lines is not only to distribute the proton beam to the horn system at a frequency of 12.5 Hz but also to deliver a beam having the optimum characteristics mandatory in the process of generating pions. The beam waist must be located in the middle of each of the targets (which are 78 cm long) and must have a regular Gaussian shape of width σ= 4 mm [10].

A beam dump will be located after the pair of bipolar kickers in order to stop the 4.5 GeV energy proton beam in case of failure of the magnets. The power of the beam to stop would be then for one single pulse (1.1×10^{14} protons) which represents 80 kW.

2.4. Beam focusing

To efficiently focus the beam onto the horn system the use of optical elements such as quadrupoles is mandatory. Quadrupoles (QP) have the function of focusing the beam on one plan and defocusing it on the other. In other words, more than one quadrupole is actually necessary to focus the beam in this present system. Several configurations have been investigated with the code TRANSPORT including two or three quadrupoles.

The transverse size and the emittances of the proton beam entering the switchyard are considered to be similar to those of the beam leaving the SPL: $\sigma = 2$ mm and the rms emittances $\varepsilon_x = \varepsilon_y = 3\ \pi$ mm.mrad (Gaussian) (Table 2). The relative errors on the emittances are considered to be 20% [22] and are included in the simulations. A 1m drift is considered between the entrance of the switchyard and the location of the first kicker. This is to foresee any eventual beam monitoring at this place to check the characteristics of the proton beam coming from the

accumulator.

The baseline configuration is **K-D-QP-QP-QP-T**. The three quadrupoles are here placed after the compensating dipole (Figure 4).
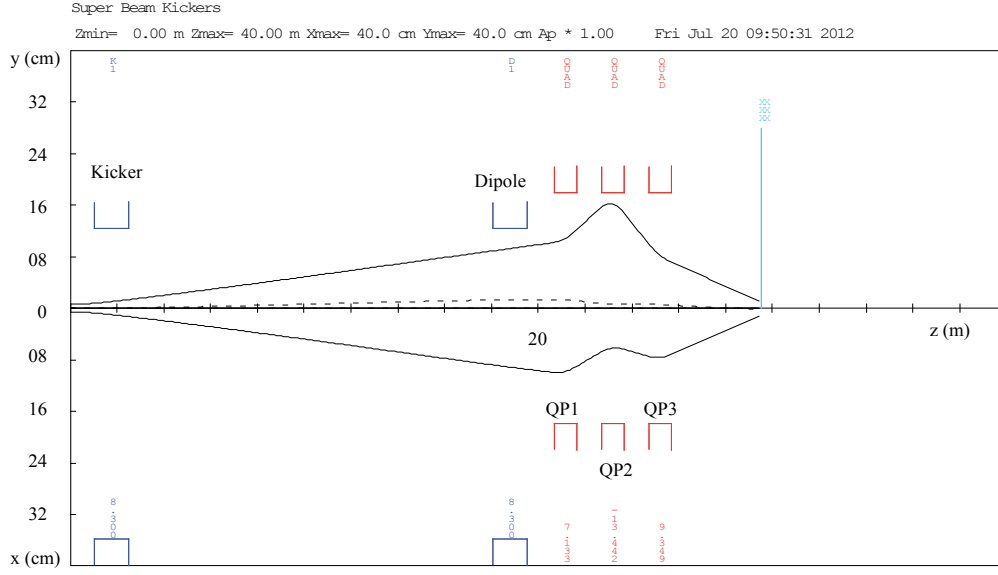

Figure 4: Transverse beam envelopes.

The beam focuses at 29.9 m (total length of the beam line and middle of the target) and its dimensions (3σ) reaches closely the values needed at this point.

The distance between:

-the 1st kicker and the target station is 29.9 m

-the 1st kicker and the dipole 1 and dipole 3 is 17 m

-the 2nd kicker and the dipole 2 and dipole 4 is 14.7 m

-the dipoles 1,2,3,4 and the target station is 11.9 m The distance from the exit of the accumulator to the entrance of the 1st kicker is assumed to be 1 m. This length is not a fixed value yet as it strongly depends on the diagnosis devices needed to control the quality and the position of the proton beam once it leaves the accumulator.

Table 3 summarizes the physical parameters calculated for the kickers, dipoles and quadrupoles for each beam line of the switchyard system. According to the high values of the intensity needed for the coils, the use of supraconducting magnets can be considered here and will be investigated in further studies.

10

	Kicker1	Dipole1,3	Kicker2	Dipole2,4
Field strength (T)	0.83	0.83	0.96	0.96
Angle of deflection (mrad)	±83.0	-	±96.0	-
Magnetic length (m)	1.5	1.5	1.5	1.5
Aperture H/V (mm/mm)	250/350	250/250	250/600	250/250
Total intensity (kA)	115.6	82.6	152.6	95.4

	Quadrupole1	Quadrupole2	Quadrupole3
Field gradient (T/m)	0.71	1.34	0.93
Aperture radius (mm)	180	180	180
Magnetic length (m)	1	1	1
Function	F	D	F
Total intensity (kA)	20.3	38.4	26.6

Table 3: Summary of the physical parameters of: kicker 1,2 and dipole 1,2,3,4 (top) quadrupole 1,2,3 (bottom) of the 4 beam lines.

2.5. *Additional beam instrumentations*

During the experiment the quality and the position of the beam must be controlled at several positions along the beam lines and mainly at the entrance and the exit point of the switchyard system. Beam collimation may be needed up stream the kicker 1 to cut off any eventual halo of the beam when leaving the accumulator. The exit point of the switchyard represents the interface with the target station and the last magnet. A consequent variation of the energy of the proton beam coming from the SPL-accumulator may also induce chromatic focusing errors within the system. The addition of sextupoles may be required to correct this effect. Beam monitors should also be added at the exit point of the switchyard to measure the transverse position of the beam and then avoid the beam from not hitting the centre of the targets as evoked in the previous section. To suppress any eventual halo from the beam and to cope with beam fluctuations (see previous section), one could consider in adding a collimator at the exit point of the system.

3. The target station

3.1. Introduction

The target station contains sets of four baffle/collimators, targets and magnetic horns within a single large helium vessel, along with the beam diagnostics and support infrastructure necessary for the safe and reliable operation of these

components. The target station is separated from the primary beamline at the upstream end by four beam windows through which enters the split proton beam. The four split proton beams pass through the collimators, targets, magnetic horns and decay volume, before being absorbed by the beam dump/hadron absorber.

The design of the target station must meet a number of important technical challenges. It requires substantial steel and concrete shielding. Due to the harsh conditions, horn and target lifetimes will be limited; multiple failures are expected during the lifetime of the facility. It is therefore essential that broken parts can be replaced, and due to the high activation this must be done using a remote handling system. It is also important that the horns and targets can be aligned with the incoming proton beams to sub millimetre accuracy. The use of four parallel horns will introduce further challenges unique to this facility. The cross section area of the beamline is increased by a factor of four, so a much larger volume of radiation shielding will be required to surround it. Having to accommodate four horns will increase the complexity of many operations, such as supporting the horns, connecting cooling and other services, replacing broken horns, and disposing of activated components.

The main objectives of the design process were as follows;

- To ensure safe operation, and compliance with all applicable radiation limits. This includes ensuring the safety of repair workers and planning for the safe disposal of radioactive scrap.

- To minimise the amount of downtime required for repairs and maintenance. This will involve increasing the reliability of components and decreasing the time taken for repairs.

- To minimise the cost of construction, operation and maintenance over the lifetime of the facility. The proposed design aims to deliver a compromise between reducing cost and reducing downtime.

The starting point for the design was the target station for the T2K experiment [24], located at the J-PARC facility in Japan. The T2K target station was designed to allow up to 4MW beam power, and has a remote handling system with similar capabilities to those required here. This is a proven design which has been running for 3 years (total $3x10^{20}$ protons on the first target), and is a valuable source of practical experience. Particular attention was paid in this new design to (i) reducing the time required to change a target or horn, and (ii) reducing the generation of tritium from the concrete within the helium volume.

3.2. Design Overview

The requirement for remote handling will be met by using an overhead gantry crane to insert and remove components from the beamline. All four horns will be mounted on a single support module which will provide support and alignment, and allow the horns to be lifted by the crane. The horns will then be moved to a maintenance area away from the beam for repair and disposal. This maintenance area will consist of the hot cell, where human operators can carry out repairs using remote manipulators, and the morgue, where activated scrap can be safely stored. In order to gain access to the components, the radiation shielding above them must first be removed. This will be achieved by making the top layer of shielding from movable concrete blocks which can be lifted off by the gantry crane. The beamline and maintenance area will be located at the bottom of a 10m deep pit in order to prevent radiation shine to the outside when moving components. The target station vessel will be filled with helium at atmospheric pressure, in order to minimise pion absorption, tritium and NOx production, and thus to provide an inert environment for the target and horns. The helium will be contained in a steel pressure vessel which will surround the horns, targets, collimators and beam dump. Beam windows will be required to separate the helium environment from the accelerator vacuum. The helium vessel will have a removable lid to allow access to the components inside.

In addition to the beamline and maintenance area, the target station must also contain the following systems;

- Cooling plant for the beamline components

- Power supply for the magnetic horns

- Air conditioning system for the buildings

- Pumps to fill and empty the helium vessel

- Control room for the crane and other target station systems

The proposed layout will consist of three buildings; a main hall containing the crane, maintenance area, and access to the beamline, a side hall containing the horn power supplies and beam dump, and a pump house for cooling and air conditioning systems. In addition to the surface structures there will be a large underground volume beneath the main hall and side hall. This will contain the beamline and maintenance area, plus shielding. The overall layout of the site is shown in figure 5.
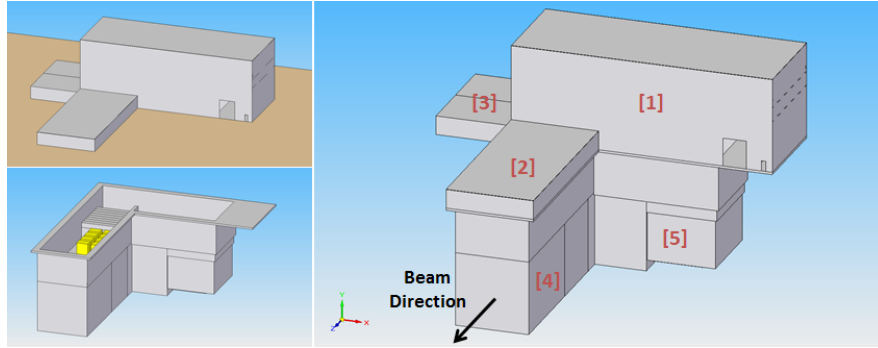
Figure 5: Site Layout; 1) Main Hall, 2) Side Hall, 3) Pump House, 4) Beamline Shielding, 5) Maintenance Area

3.3. Helium Vessel

The horns, targets, collimators, decay volume and beam dump will be contained in a steel vessel filled with helium at atmospheric pressure. Figure 6 shows the area covered by this vessel. Using helium will avoid the problems caused by passing a proton beam through air, such as the production of nitric acid which causes steel embrittlement, and the activation of large volumes of air. Using helium rather than a vacuum will allow for cooling of components by conduction and convection, and will prevent stresses in the vessel due to differential pressure. However, the vessel will be required to temporarily withstand vacuum pressure as it will be vacuum pumped and then back-filled with helium in order to achieve a high helium purity. The split proton beam will enter via four beam windows which will separate the helium vessel from the accelerator tunnel. The beam windows will connect to both sides via inflatable pillow seals, as used in T2K [2]. The benefit of pillow seals is that they can be remotely disconnected and do not depend on a mechanism to operate, so a damaged beam window can be replaced without requiring complex tooling or exposing a human repair worker to radiation. All four beam windows will be mounted on a single frame which can be lifted out by the gantry crane after the pillow seals have been disconnected. The hot cell will then be used to replace the damaged window without having to scrap the whole frame.

The helium vessel and the decay volume will be joined to form a single pressure vessel, as in T2K. As a result, the entire decay volume must be pumped out every time the helium vessel needs to be opened in order to replace a component. Running the four targets at full power will cause a predicted heat load of 511kW
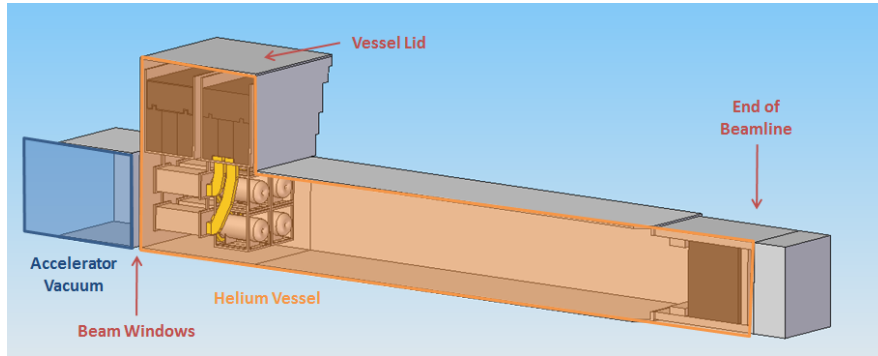
14

Figure 6: Extent of Helium Vessel

on the walls of the helium vessel and decay volume due to secondary particle interactions. As a result the walls will require active cooling, which will be achieved by using water channels on the outside of the vessel as for T2K.

3.4. Support Module

The horns and collimators will be held in place by support modules which can be lowered vertically into the helium vessel by crane, as shown in figure 7. One support module will hold the four horns, and a second will hold the four collimators. The support modules rest on kinematic mounts at the top of the helium vessel. Removable shield blocks will fit inside the support modules, and rest on the sides of the vessel. The sides of the shield blocks will be stepped to create a labyrinth, preventing direct shine of radiation to the top of the vessel. The easiest place to disconnect services will be immediately after the feedthroughs, just inside the vessel. This will allow the connection points to be accessed from the top of the vessel without having to remove the shield blocks first. A mechanism for quickly disconnecting striplines has been developed by Fermilab, and a similar design could be used here.

3.5. Horn Alignment

It is essential that the four horns containing the four targets can be aligned with the four proton beams to sub millimetre accuracy. This will depend on the alignment of the horns relative to the support module carrying them, and the alignment of the module relative to the helium vessel. This will be achieved by having the support modules rest on kinematic mounts, which are designed to exactly constrain the six degrees of freedom of motion. The kinematic mounts will allow
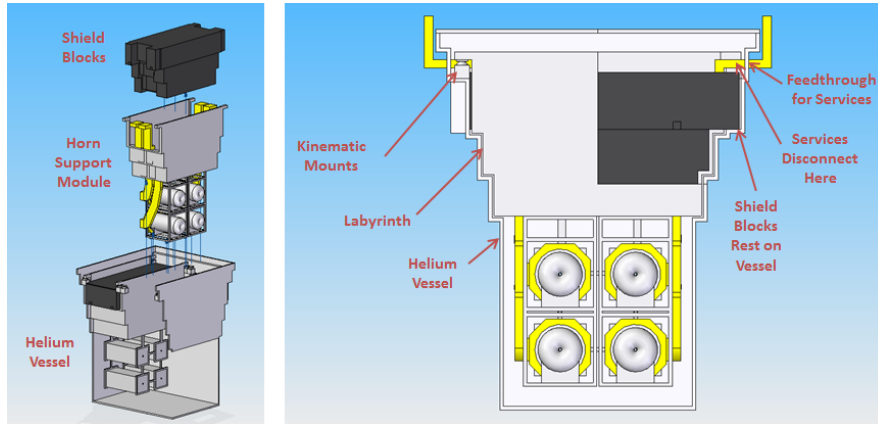
15

Figure 7: Support Modules, Shield Blocks and Helium Vessel

the position of the module to be precisely defined in relation to the helium vessel, with high repeatability.

3.6. Horn Power Supply

Power for the magnetic horns will be provided by 8 power supply units (PSUs) connected to the horns by striplines. The length of stripline required should be minimised in order to minimise electrical losses. However, the PSUs must be located outside the radiation shielding to protect them from damage. This will be achieved by locating the PSUs on top of the decay volume shielding. This ensures the PSUs are as close as possible to the horns. Above the beam dump shielding there will be space available for broken PSUs to be moved for maintenance. A 5 tonne gantry crane in the side hall will be used to carry the PSUs.

The power supply is designed so that every horn must be connected to every PSU. The length of stripline must be roughly the same to each horn in order to ensure accurate timing, which is made more difficult by the fact that the lower horns will be further from the supply. Figure 8 shows the stripline layout which was designed to solve this. The length of stripline between the end of the PSUs and each horn is 20m, which is less than the specified maximum length. Each horn must be powered in turn as the beam is cycled around the four targets. Figure 8 shows which stripline connects to each horn, and also indicates the order in which the horns will be powered.
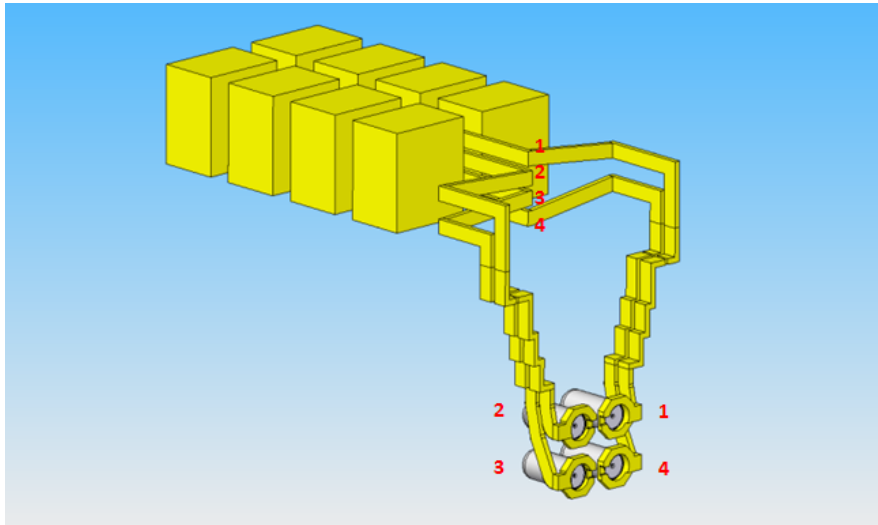
Figure 8: Stripline Connections from PSUs to Magnetic Horns

3.7. Hot Cell

The hot cell will consist of a safe containment area for activated components and a shielded operator room. Repairs can be carried out by a human operator using remote manipulators to safely work on highly activated components. Two lead glass windows positioned at 90 to each other provide direct visibility. The crane could be used to lift and rotate the component by 180, in order to give a complete 360 view. Access to the hot cell will be via a shaft from the control room building, allowing the hot cell to be accessed without having to enter the main hall. The roof of the hot cell will consist of removable concrete shield blocks, so it can be sealed when not in use. The roof of the operator room will also be made from shield blocks to allow for easy installation of manipulator arms using the main crane.

3.8. Morgue

The morgue will consist of a large underground space in which broken parts can be stored until their activation level has dropped enough that they can be moved elsewhere. Components in the morgue will be sealed in steel casks to stop most of the radiation. In addition to the casks, the morgue will be shielded by concrete walls on all sides. The morgue size specified here will have enough

space to contain 6 complete support module assemblies, although one of these spaces will be filled by the spare horn assembly.

3.9. Shielding

The main source of radiation will be the horns and targets. To provide a biological shield, the helium vessel will be surrounded on all sides by a 2.2m thick iron inner shield followed by a 3m thick concrete outer shield. The rest of the beamline will be less active, and will be surrounded by a 5.2m thick concrete shield. The maintenance area will also require shielding, around 2m of concrete on all sides. Based on previous experience, it is recommended that low sodium concrete be used for the shielding, to limit the formation of radioactive sodium isotopes in the shielding. The outer concrete shield will need to be sealed to prevent activated air leaking from the region immediately surrounding the helium vessel into the target station atmosphere. There must be some way to open the shielding in order to gain access to the components inside. This will be achieved by making the top of each shield out of stacked concrete blocks which can be moved by the crane. Figure 9 shows the shielding arrangement around the beamline.
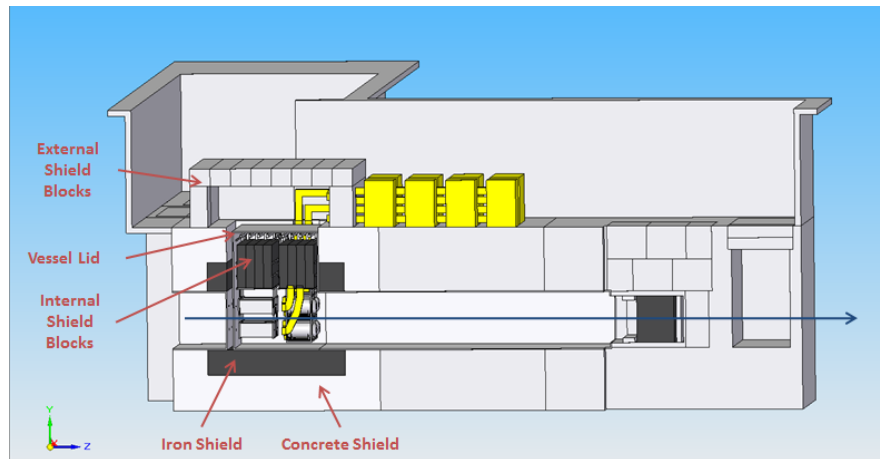

Figure 9: Beamline Shielding

3.10. Crane and Control Room

Activated components will be moved using a 100 tonne gantry crane. This crane will also be used for initial installation of components and for moving replacement parts into the target station. There will also be a 5 tonne gantry crane in
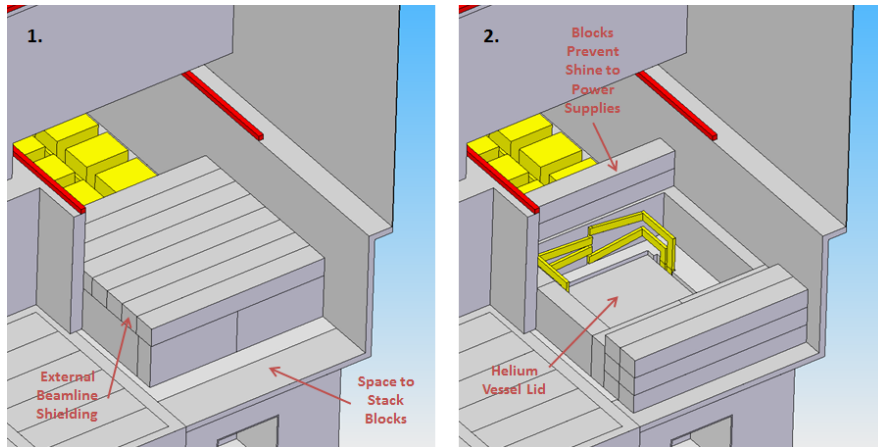
18

Figure 10: External Shielding of Helium Vessel, 1) Closed and 2) Open to Access Vessel

the side hall, for carrying power supply units. The 5 tonne and 100 tonne cranes will overlap, so that the PSUs can be delivered to the main hall, unloaded by the large crane, then transferred to the small crane to be installed in the side hall.

3.11. Maintenance Procedure

To minimise downtime, two assemblies of four horns each will be used at any one time. This will allow one assembly to be repaired while the other is running, so the beam will only have to be stopped for long enough to exchange the assemblies. The spare assembly will still be fairly active, and will therefore be stored in the morgue for safety. A procedure for a standard repair operation, for example replacing a broken target, has been studied.

3.12. Decay Volume and Beam Dump

The decay volume will consist of a 25m long steel pressure vessel connecting the target station helium vessel to the beam dump. It will be directly connected to the helium vessel and so will also be filled with atmospheric pressure helium. The entire vessel will be built to withstand a vacuum when the helium is pumped out. The decay volume will be shielded with 5.2m thick concrete on all sides. The steel vessel will experience significant heating from particle interactions and will therefore require its own cooling system. The beam dump will be a large, externally cooled block of graphite similar to T2K. It will be in the same helium environment as the horns and decay volume. It will be housed in a steel pressure

19

vessel which is connected directly to the end of the decay volume. The design of the beam dump itself will be covered in detail in section 6.

Downstream of the beam dump will be a pit to house muon monitors if required. Access to the pit will be via a staircase in the side hall. If they are not required then this area can be omitted and the side hall shortened.

4. The target

For the EUROnu Super Beam facility a high power target is required to generate pions to be focused by a magnetic horn. The target is expected to withstand the beam induced heating and associated stresses as well as offer reliable operation whilst exposed to intense radiation. The main technical challenges are as follows:

1. Heat removal. A significant heat load is deposited by the beam on the target and has to be removed reliably by the cooling system.
2. Static and dynamic stresses. The target must withstand thermal-mechanical stresses arising from the beam induced heating of the target.
3. Radiation damage. Degradation of the material properties due to radiation damage must be accommodated.
4. Geometrical constraints. The target has to fit inside the bore of the magnetic horn whilst having an appropriate geometry for effective pion production.
5. Remote replacement. Once activated the target has to be remotely manipulated in the event of failure.
6. Minimum expected lifetime. The target is expected operate without intervention between scheduled maintenance shutdowns.
7. Safe operation. The target design should minimise any hazard to the personnel or the environment

In the proposed concept, the target stands alone from the magnetic horn, has its own cooling system and can be removed and replaced remotely. A combined target and horn design has also been considered but was rejected in favour of a separate target and horn system. The reasons for this decision are discussed in section 4.1. Several target technologies have been considered and the two most favourable concepts are presented in the following sections.

4.1. Design philosophy

Two outline target design concepts have been considered, namely

1. a combined target and horn inner conductor,

2. a separate target and inner conductor, with the target supported within the horn bore.

Studies have shown that the latter of these two options is preferable and this has been adopted as the baseline. A separate target and horn inner conductor was found to be preferable for the following reasons:

1. Removing the beam heating of the target and the Joule heating of the horn are both significant challenges. Separation of the two items reduces the challenge and permits separate cooling solutions.
2. More favourable target designs and cooling options, including segmented targets are possible, since the target is not required to conduct the horn current. A segmented target offers increased tolerance to accidental off-centre beam conditions.
3. The thermal stress in the target is reduced without the additional joule heating from the horn current pulse
4. An increase in the horn inner conductor radius is possible, which significantly reduces the magnetic stress
5. It becomes possible to tune the target and horn geometry separately, both radially and longitudinally, which permits greater scope for optimization of the neutrino yield
6. Failure modes are not combined, possibly leading to longer lifetimes for both target and horn
7. Targets can be replaced separately within the horn, reducing cost of replacement and quantity of radioactive waste.

4.2. Target Cooling

A 1 MW proton beam with a kinetic energy of 4.5 GeV deposits of the order of 50 kW of heat in a low-Z target. Both contained water and helium gas cooling have been considered.

Helium cooling is preferred because there is negligible interaction between the beam and coolant making it readily possible for the coolant to be within the beam footprint for more direct cooling of the target. Beam induced pressure waves in a gaseous coolant are largely reduced if compared with a liquid coolant, little activation of the helium is expected and there are no corrosion issues with the target and cooling circuit materials. Several different target cooling geometry options are possible. Challenges or disadvantages of helium cooling compared with water include the fact that a relatively high pressure (larger than 10 bar) is required to

generate a sufficient mass flow whilst limiting gas velocity and pressure drop to acceptable levels.

4.3. Thermo-mechanical design of the target

4.3.1. Packed Bed of Titanium Spheres

A packed bed of target spheres has been considered because of its inherent lower quasi static and inertial dynamic stresses. The packed bed target is made up of a canister containing many small target spheres. The packed bed canister has dimensions of the same order as the monolithic target but the individual spheres are much smaller. This has three advantages in terms of stress:

1. The spheres are almost uniformly heated by the beam because of their size and have a much shorter conduction path from the centre of the sphere to the cooled surface. This means the temperature gradients in small spheres are small with respect to a larger monolith of the same thermal conductivity. The quasi static stresses are driven by the temperature gradient and they are correspondingly lower.
2. The expansion time of a small sphere is much shorter than that of the solid monolith of the same material. In the case of the monolith the expansion time is longer than the pulse duration and as such significant inertial stresses occur. With small spheres the expansion time can be less than the pulse duration and so inertial stresses as a result of rapid energy deposition are negligible.
3. In the event of an off-centre beam hitting a target an asymmetric temperature profile is set up. This will have the effect of bending a solid monolith target and producing additional stress oscillations. As the spheres in a packed bed are not connected to each other and experience a close to uniform energy deposition whether the beam is on centre or not the packed bed configuration is inherently insensitive to an off centre beam.

Compared to the solid monolith target the packed bed has a lower density. Beryllium has been considered for the solid target which has a density of about 1.85 g/cc. Depending on the packing of the spheres the packed bed may have a bulk density of between 0.5 and 0.74 of the solid density. The density of the target material has an important effect on pion yield and so in order to recover the bulk density loss titanium which has a density of 4.5 g/cc is proposed as a candidate material. A comparable pion yield from the surface of a solid Beryllium target and a 50% density Titanium target has been demonstrated using detailed simulation.

A Titanium packed bed with packing factor of 0.74 has been evaluated from a physics point of view with favourable results.

The packed bed canister would have a diameter just larger than the upstream baffle to protect it from a direct hit from the beam. It would be surrounded by coolant flow channels and would be perforated to allow the coolant to pass through the centre of the spheres. This configuration gives rise to significantly more surface area for heat transfer than is present with the monolith target. The ideal flow configuration is transverse, i.e. the coolant passes through the packed bed in a direction perpendicular to the beam (Fig. 11). This minimises pressure drop and so allows a greater volume flow through the target. As with all solid high power targets that are gas cooled an advantage can be gained by pressurising the coolant. This allows an increase in mass flow without increasing the required pressure drop to drive the gas through the target.
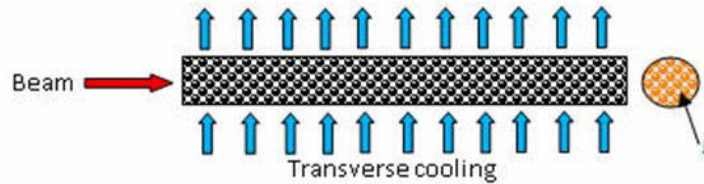

Figure 11: Packed Bed ideal flow configuration.

The larger surface to volume ratio with respect to the monolithic target and the proximity of the coolant to the core of the target offers potential for greater heat dissipation. Coolant gas is preferred over liquid due to complications associated with a liquid passing through the beam.

4.3.2. Packed Bed Model

An example case of a packed bed of Ti6Al4V spheres with transverse flow has been modelled. Energy deposition in the spheres has been calculated from a FLUKA model of a titanium solid target with half density. Titanium has better thermal conductivity than its alloys but some alloys such as Ti6Al4V have much higher strength and as such has been chosen for this example. Obtaining a practical transverse flow configuration within the confines of the magnetic horn is not trivial however a scheme is described here and some preliminary conjugate heat transfer modelling (using CFX) on an example case with a 1 MW beam has

been carried out. (Figures 12 and 13 show some plots from the model). The geometry involves three inlet and three outlet channels spread at 120° around the canister (Fig. 12). Holes of various sizes are strategically placed in the canister to allow gas to flow through the packed bed. The packed bed is modelled as a porous domain and appears to act as a diffuser with the flow naturally dividing evenly throughout the porous domain. The pressure drop in the porous domain is calculated using the Ergun equation [25] i.e.

$$\Delta P = \frac{f_p \rho V_s^2 (1 - \epsilon) L}{D_p \epsilon^3},$$ (1)

where f_p is a function of the packed bed Reynolds Number, ρ is the density of fluid, V_s is the superficial velocity, L is the length of the bed D_p is the equivalent spherical diameter of the packing, ϵ is the void fraction of the bed.

A mass flow of helium of 93 g/s is used with an outlet pressure of 10 bar. The pressure drop in the packed bed itself seems perfectly manageable and it appears as though there is scope for higher flow rates. Experience so far indicates that flow in the channels and in particular through the holes into the packed bed is the most significant cause of pressure drop. However the predicted pressure drop of 1.1 bar appears reasonable and little design optimisation has yet to be put into this example case. The maximum helium temperature is 584 °C although the average outlet temperature is only 109 °C. This difference is due to the energy deposition in the packed bed not being uniform. The maximum sphere temperature is calculated to be 673 °C (Fig. 13). The maximum steady state (ignoring temperature jump) sphere temperature, T_c, depends on the size of the sphere, D_p, conductivity of the sphere material, k, and the surface temperature, T_s, i.e. (appendix).

$$T_c - T_s = \frac{Q(D_p/2)^2}{6k}$$ (2)

where Q is the energy deposition (W/m3). The surface temperature depends on the heat transfer coefficient between the coolant gas and the sphere. This is calculated from a Nusselt number correlation for heat transfer in pebble beds with high Reynolds number [26]

$$Nu = [(1.18Re^{0.58})^4 + (0.23Re^{0.75})^{0.25}$$ (3)

The three outlet channels are common and are configured such that the structure does not experience any significant asymmetries in its temperature profile.

Below follows a list of the key areas that need further work for the development of the packed bed target concept.
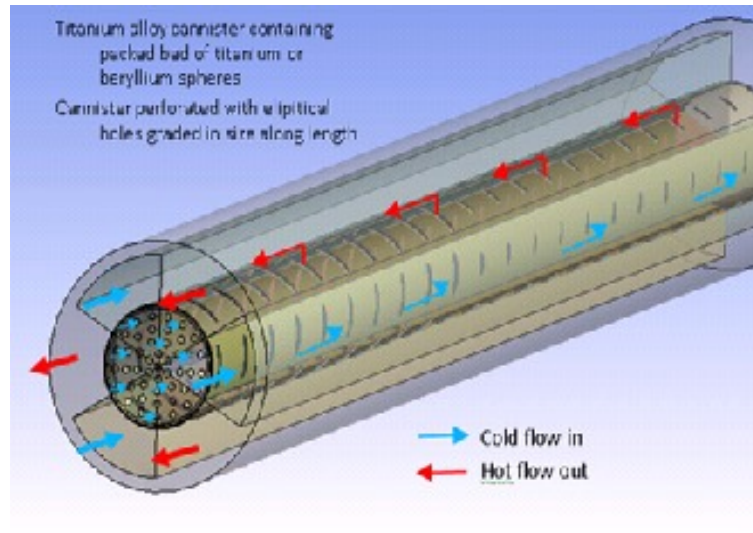
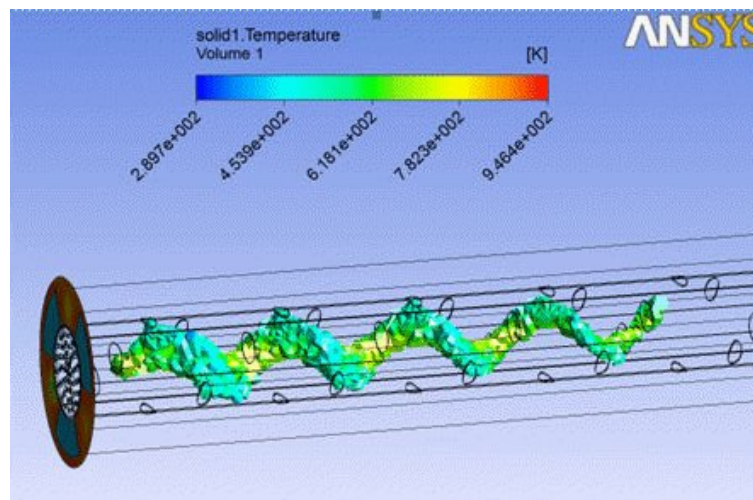Figure 12: Proposed Packed Bed Flow.

Figure 13: Maximum sphere temperature.

1. The requirement for pressurised cooling gas necessitates a beam window that can withstand the pressure difference between a vacuum and the coolant pressure.

2. Slight movements between the packed spheres may occur as a result of the sudden temperature jumps and corresponding thermal expansion. The titanium spheres with the highest energy deposition will have a temperature jump of 83 °C with a 1 MW beam.

3. If the beam pulse is much shorter than the expansion time of the spheres this could give rise to an additional shock stress (assuming instantaneous heating). However the expansion time of the spheres is very small (a fraction of a microsecond) with respect to a solid monolith target so these inertial stresses are likely to be less important. None the less this should be checked.

4. The canister would need to accommodate the thermal expansion of the target spheres.

5. The beam must pass through the canister to enter the packed bed, a perforated cooled plate is envisaged to enclose the spheres while allowing coolant to pass through so as to minimise temperature gradients in the perforated plate. Stress analysis of this component is required.

6. Off-centre beam effects on the packed bed canister should be evaluated.

7. A higher flux of neutrons is expected from the titanium packed bed with respect to the beryllium monolith. This may have a detrimental effect on the horn and needs to be investigated.

4.3.3. How much heat can be removed from a packed bed?

The limiting factors for the heat dissipation capability of a packed bed are the coolant exhaust temperature, the coolant pressure drop across the target and the peak temperature and stress in the target spheres. For this 1 MW example modelled here it appears there is some head room in terms of the key limiting factors, one may even be bold enough to say that a target capable of dissipating a multi megawatt beam may be possible. This has been claimed for the case of a high Z packed bed by Sievers and Pugnat in the past [27]. In order to find the practical limit of a packed bed some further analysis and CFD is required.

5. The horn

5.1. Hadrons focusing system: the electromagnetic horn

In the case of the CERN SPL Super-Beam (SB) the operation conditions of the horn will be much more severe than in previous applications. Table 4 shows a

comparison of some horns already used by past or ongoing projects. In this table one can see that this horn has a small length which could be an advantage during the fabrication and operation, but, on the other side, the proton driver power (4 MW) and repetition rate (50 Hz) are considerably higher than other applications, a real challenge!

Table 4: Comparison of horns.

Project	Proton Energy (GeV)	Power (MW)	Rep. Rate (Hz)	Current (kA)	Number of horns	Length (m)
CNGS	400	0.2	2 pulses/6 sec	150	2	6.5
K2K	12	0.0052	0.5	250	2	2.4–2.7
NUMI	120	0.4	0.5	200	2	3
MiniBoone	8	0.04	5	170	1	1.7
T2K	50	0.75	0.3	320	3	1.4–2.5
SPL-SB	3.5-5	4	50	300–600	1-2	1.3

5.2. Horn design

An initial design of a horn prototype system (horn+reflector) [3, 4] foreseen for a neutrino factory (NF) has been made at CERN for a 2.2 GeV proton beam. An optimization and a redesign has been made in a SB context [8, 28], driven by the physics case of a long baseline experiment (130 km) between CERN and Fréjus (MEMPHYS detector location).

New studies of a hadron focusing horn have been done and as a result an optimal closed forward geometry with non integrated target has been designed [29] , [30], shown in Fig. 14 and with geometric parameters reported in Table 5. In summary, high magnetic field closed to the target and small material thickness are desirable to obtain the best meson focusing and minimize multiple scattering and secondary particles interactions [31].

Given the nominal values of the proton beam power $P = 4$ MW and current $I_0 = 350$ kA, a high power density is present inside the target and horn wall conductors. The feasibility of this horn design depends mainly on the temperature and stress level inside the target and horn structure. The stress level needs to be compared to the fatigue strength of the material to give an estimate of the horn lifetime.

The horn will be made of Aluminium AL 6061-T6 with 3 (10) mm thickness for the inner (outer) conductor. The horn is approximately 2.5 m in length and 1.2 m in diameter. For the horn assembly, the different parts will be welded at different
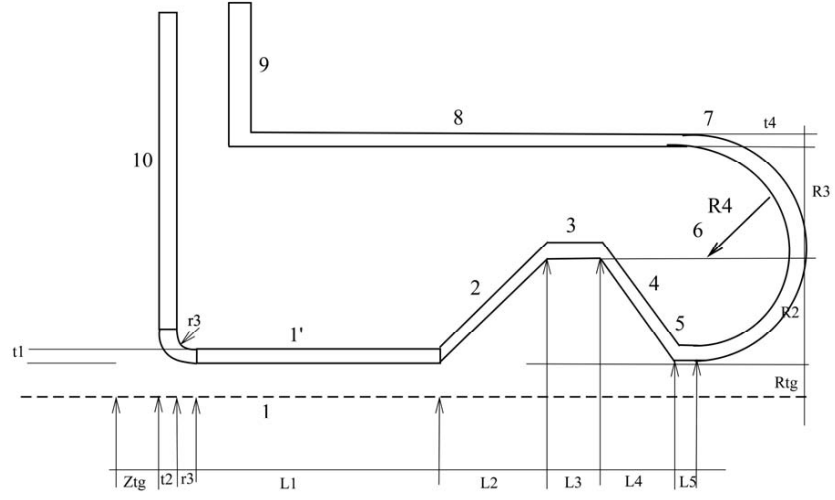
Figure 14: Horn parameters

Parameters	value [mm]
L_1, L_2, L_3, L_4, L_5	589, 468, 603, 475, 10.8
t_1, t_2, t_3, t_4	3, 10, 3, 10
r_1, r_2	108
r_3	50.8
R^{tg}	12
L^{tg}	780
z^{tg}	68
R_2, R_3	191, 359
R_1 non integrated	30

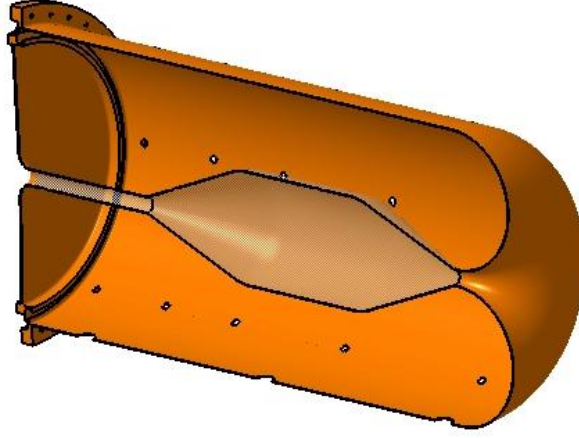Table 5: Horn geometric parameters.

Figure 15: Cross section of the horn.

locations, preferably in the low stress regions. The inner and outer conductor end plates are electrically insulated with a glass disk of 2.5 cm thickness. The target with its own cooling system will be inserted inside the central hole of the horn with an inner diameter of 6 cm. Spacers will have to be designed to maintain the target inside the horn.

In the following sections we present the electrical, thermal and mechanical studies of the electromagnetic horn.

5.3. Electrical currents and magnetic flux

An analytic calculation for the toroidal magnetic field in the horn created by the alternate current has been performed. Most of the current inside the inner conductor is flowing in the region $3.1 < r < 3.3$ cm, accordingly to the calculated skin depth. Electrical losses occur in the inner conductor, conical sections and at the top end of the horn.

5.4. Thermal loads and cooling

In steady state and from the power density distribution, it is possible to calculate the required heat transfer coefficient h to maintain a temperature difference $\Delta T = T_{horn} - T_{inf} = 40\,^{\circ}C$. The cooling efficiency of the system required to maintain a constant temperature inside the horn structure is proportional to the thickness wall e and the power density q.

29

The temperature distribution has been computed for a basic cooling scenario of $\{h_{inner}, h_{horn}\} = \{1, 1\}$ kW/(m^{2}K) and for an optimized cooling scenario with higher cooling in the hot spot area $\{h_{inner}, h_{corner}, h_{conv}\} = \{3.8, 6.5, 0.1\}$ kW/(m^{2}K). h_{inner}, h_{corner}, h_{conv} being the heat transfer coefficient on the surface of the inner conductor, on the upstream bottom corner (near the target) and on the right side of the upstream bottom plate.

The high heat transfer coefficient seems to be quite challenging as it requires a high water flow [33]. Further developments are required on the basis of commercial nozzles and tests in order to increase the conventional capacities [34, 35]. Nevertheless, heat transfer coefficient in the range of 10 kW/(m^{2}K) can be expected at flow rate of approx. 4 l/min with the help of the micro-channel technique developped for VLSI chips at Soreq [36].

For the uniform cooling, the maximal temperature is $180\,^\circ C$. When higher cooling is used in the hot spot area, the maximal temperature is $61\,^\circ C$. The water jet nozzles disposition and individual flow rates of the jets will have to be chosen according to these h coefficients required to maintain a reasonable maximal temperature around $60\,^\circ C$. This thermal model shows that the two hot area are the upstream bottom corner and the downstream part where the inner radius becomes $r = 3$ cm. These two domains will have to be cooled very well to avoid any failure.

5.5. Static mechanical model

The displacement field has been computed and shows a maximal displacement of $u_{max} = 1.12$ mm occurring in the downstream part of the horn (opposite to the target side).

The maximal stress of 62 MPa occurs in the corner region. This value is well below the aluminium maximal strength but still high in comparison of Al 6061 T6 fatigue limit for 10^8 cycles. There is also a high stress level in the top inner waist of the horn. This part and segments junctions will require some slight modification to achieve a stress as low as possible below 20 MPa for example. This static thermal stress is due to thermal gradient due to non uniform temperature distribution inside the horn.

It is interesting to note that the static stress level can be greatly reduced to 6 MPa if we achieve a uniform temperature. The displacement is about 2.4 mm when the horn submit to uniform thermal dilatation with $\Delta T = 40^\circ C$.

5.6. Transient mechanical model

The transient stress from the magnetic pressure pulse is significant mainly for the inner conductors of the horn with small radius such as the inner conductor parallel to the target and inner waist in the downstream region.
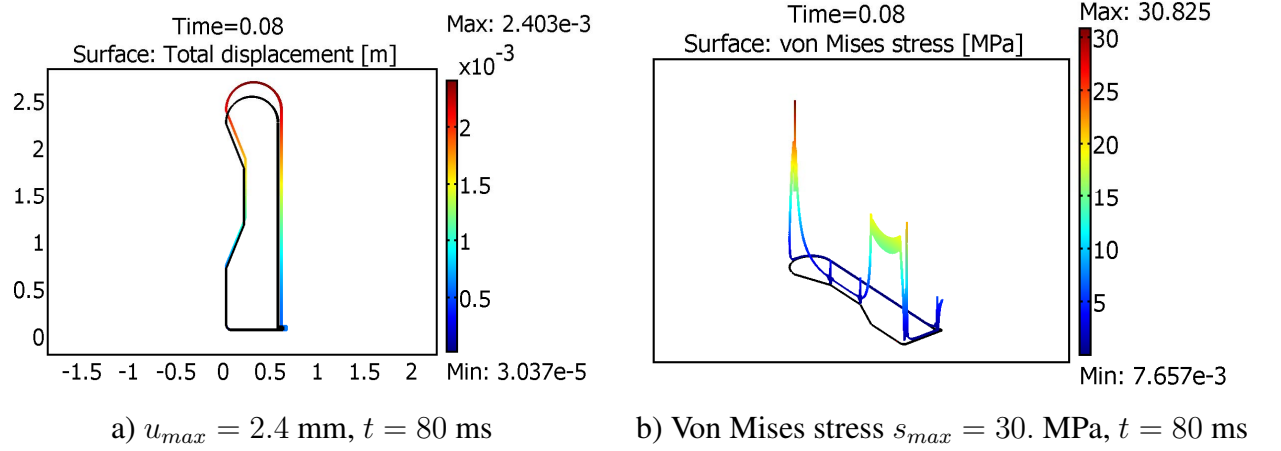

a) $u_{max} = 2.4$ mm, $t = 80$ ms   b) Von Mises stress $s_{max} = 30.$ MPa, $t = 80$ ms

Figure 16: Displacement field a) and von mises stress b) due to thermal dilatation with uniform temperature $T_{horn} = 60°C$

The displacement is maximum in the top part of the horn (dowstream region, Fig.16). The displacement due to the magnetic pulse is quite low in comparison to the thermal dilatation. The von Mises stress is the highest in the upstream corner region. The magnetic pressure pulse contributes for about 20 MPa in the top part of the horn region with $r = 3$ cm.

The thermal dilatation does not contributed to the radial stress but mainly to the longitudinal stress S_z as expected. The thermal static von Mises stress is about 2.5 MPa and the peak stress is 15 MPa. Because the inner conductor thickness $e = 3$ mm is small compared to the inner radius $r_i = 30$ mm the hoop stress inside the inner conductor is approximately constant with a value of 19 MPa.

5.7. Cooling system

The heat sources are: electrical resistive losses from pulsed currents and secondary particles generated from the proton beam/target interaction. The heat transfer coefficient depends on the two water phases, the flow rate, the geometry, and the disposition of the nozzles. Assuming a initial inlet temperature and outlet temperature $\{T_i, T_{outlet}\} = \{20, 60\}°C$ and a total power to removed of
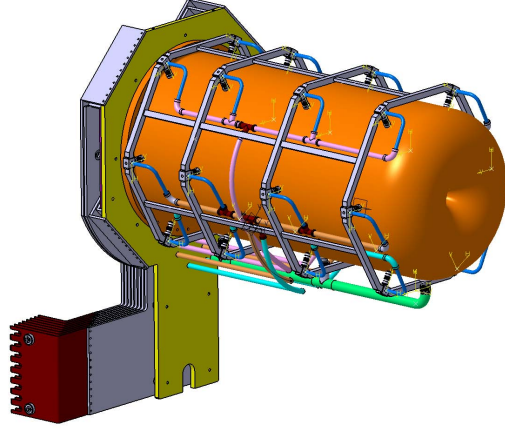
Figure 17: Horn with striplines and cooling system.

$Q = 22 + 40 = 62$ kW, the water mass flow rate is 0.37 kg/s. Hence, assuming ideal heat removal the minimum water flow rate will be 24 l/min. The final flow rate can be estimated to be in the range of $60 - 120$ l/min per horn. The flow rate and jets characteristics will be chosen in order to limit the conductors temperature below a safe limit around $60\,°$C and to remain in a single liquid phase cooling regime. To minimize possible failure or water leaks, it is preferable to minimize the number of jets. Currently, 6 jets are located in the circumferential direction covering an angle of $60°$ each with 5 rows giving 30 jets in total.

5.8. Modal analysis, natural frequency

The current pulse circulating inside the horn is of sinusoidal form with a $100\,\mu s$ width. The repetition frequency is 12.5 Hz in normal use with a 4 horn system or 16.6 Hz with 3 horns running. The first six eigenfrequency for this current horn geometry are $f = \{63.3, 63.7, 88.3, 138.1, 138.2, 144.2\}$ Hz excluding all the pipes and the frame connected to the horn outer conductor. The first 3 fundamental modes are related to the inner conductor vibrations, the fourth, fifth and six modes are related to the outer conductor vibrations.

5.9. Fatigue limit for Aluminium

The design life of the horn should be intended for 10^9 pulses which is about 926 days lifetime. There is no fatigue limit for Aluminium alloy, which means that fatigue data can only give a probability of failure for a determined level of

stress and number of cycles. In the MiniBooNE design horn[37] the maximum equivalent stress limit used is 68 MPa everywhere in the horn to have a 97.5% confidence level for no failure at 10^8 cycles.

The presence of an initial mean stress such as mean stress due to thermal dilatation reduces the fatigue strength [38, 39].For sustained cyclic conditions, the material should stay in the elastic regime or in other words any combination of mean stress and alternating stress should not create yielding or plastic deformation. According to reference [32], the fatigue strength limit are $\{20, 50\}$ MPa for 10^9 pulses for zero and with a maximum mean stress respectively. For the weld junction with mean stress a limit of 10 MPa should be used.

For the inner conductor horn, the magnetic pressure pulse creates a peak on the von Mises stress value of about 16 MPa. This value is below the 20 MPa limit strength for 10^8 cycles and with mean stress due to thermal dilatation [40, 41].

5.10. Effect of neutrons irradiations

In the case of high neutrons flux, ($> 6 \times 10^{22} n/cm^2$) the formation of He and H creates cavities and bubbles inside the materials. These defaults lead to a reduction of the mechanical properties of the material [42]. Nevertheless, Fluka simulations shows that the neutrons flux through the horn is much lower than $10^{22} n/cm^2$, so the material properties should not be degraded by neutron irradiation. The mechanical properties of the Aluminium alloy 6061-T6 may change under irradiation of all the secondary particles generated from the proton beam and target interactions and their synergy with the applied stresses [43, 44]. For moderate neutrons flux the neutrons create the transmutation of Al_{27} to Si_{28}. This can lead to the formation of Mg_2Si precipitate and an increase of the yielding strength (limit of elasticity) and the ultimate tensile strength. Radiation hardening generally decreases the tensile elongation (depending on the alloy). This issue has to be investigated in order to evaluate the impact on the material resilience in the case of fatigue stress. A first evaluation of the resultant dpa due to irradiation along the longitudinal beam axis revealed a peak value of 10^{-5} dpa [41, 45, 46]. Taking into account the mechanical stress cycles leads to an additive formulation which integers all the micro-damages (microvoids, microcracks, clusters, etc.). The resultant number of micro-damages is 0.1 for 10^4 cycles.

Although multi-physics simulation of the whole system can greatly help the conception of a reliable design, a dedicated R&D and testing with a target will be needed in the future to validate these studies but also to face the various safety aspects (chemistry of heavy metals, high radiation levels, high voltage,high cur-

rent...), which would also include the design of a complete remote handling installation for the horn and target maintenance and possible exchange.

5.11. The horn power supply

To provide the $\frac{1}{2}$ sinusoid waveform current to a horn, we have studied a power supply. A capacitor charged at +12 kV reference voltage will be discharged through a large switch in a horn via a direct coupled design. A recovery stage allows to invert rapidly the negative voltage of capacitor after the discharge, and to limit the charge capacitor current.

We have adopted a modular architecture with 8 units (Fig. 18): 2 modules are interconnected on a same transmission line based on 2 strip-lines (Rtl=1.683 mΩ and Ltl=435 nH). To limit energy consumption and therefore current delivered by the 12kV capacitor charger, investigations have been done to reduce the resistivity and the inductance by studying a transmission line based on large strip-lines of aluminium. It allows to obtain a small resistivity of 51 $\mu\Omega$/m and 13.2 nH/m for 2 plates (0.6 m high X 1cm width) and spaced by 1 cm.

The capacitor charge and recovery circuits operate at 50 Hz, the discharge of current in each horn accurs at a 12.5 Hz frequency and is delayed by 20ms between each horn.

The power delivered by the capacitor charger attains 70.8 kW rms per module, that is 566 kW rms in total. It represents only 3% of quantity of current discharged in horn, so the recovery energy efficiency is very high and recovers 97%. A sketch of one unit is shown in Fig. 20. A more detailed description of this device can be found in [47] and [1].

5.12. The target and horn support structure

A supporting structure for the targets and the horns has been studied in detail. A sketch of this structure is shown in Fig. 21. An optimization has been conducted by modifying the thickness of the beams to offset the frequency of the second mode from the excitation frequency. More detail can be found in xx.

6. Studies of activation and shielding

6.1. Simulation technique

A detailed calculation of the tqrget and horn activation has been realized with FLUKA [48, 49] version 2011.2.7 in order to study the activation of the target and horn and to determine the thickness of shielding required to comply with the radiological regulations.
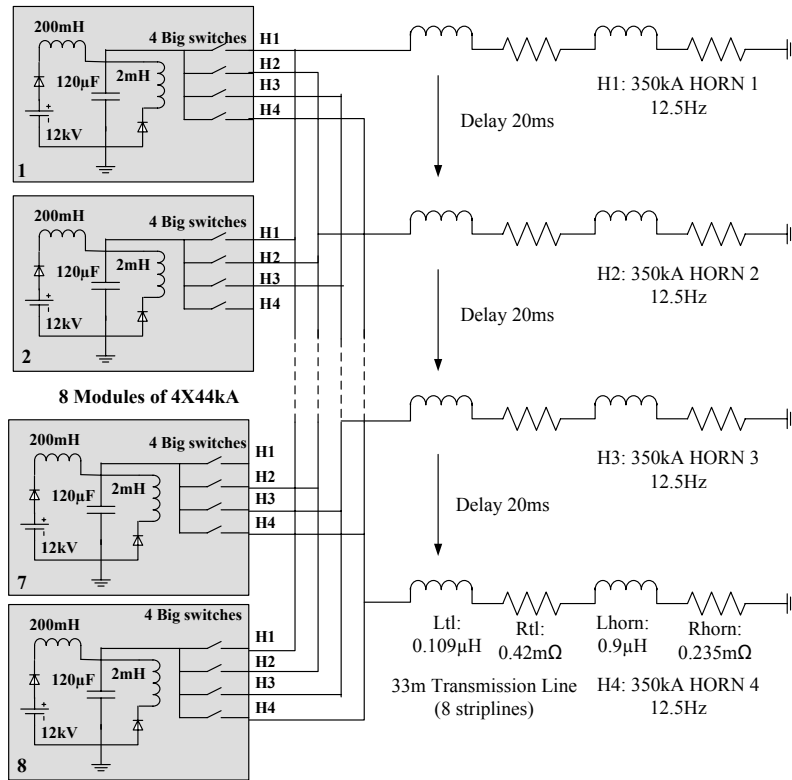
34

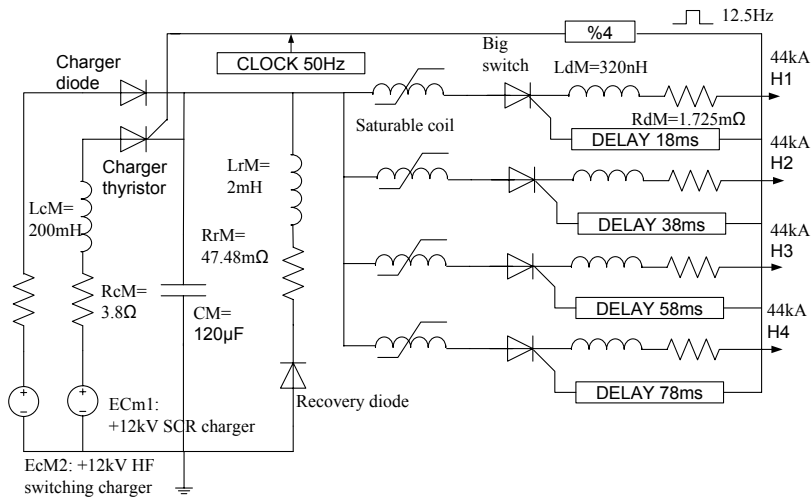Figure 18: Modular architecture of the horns power supply.
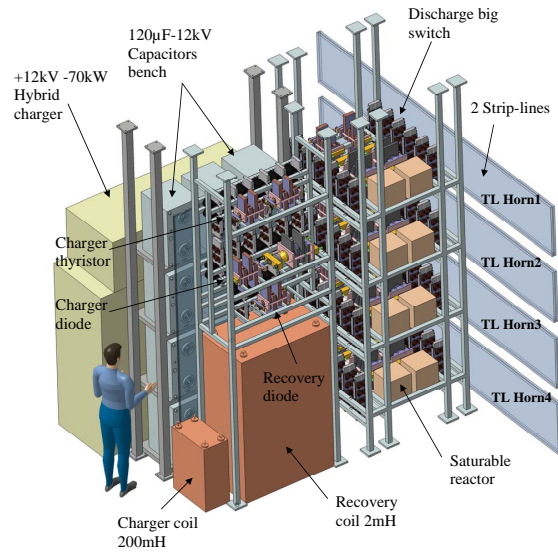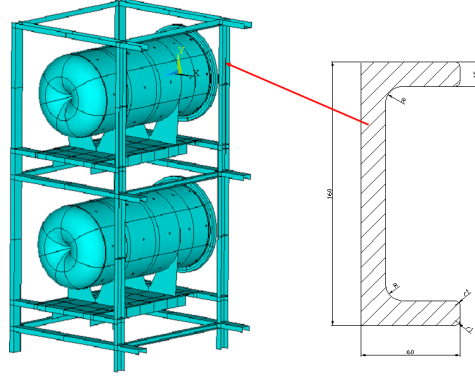
Figure 19: Diagram of a power supply module.

Figure 20: Sketch of a power supply unit.

Figure 21: Symmetric half of four horn assembly with detail of channel section used for supporting frame

The calculation have been done by considering 200 days of irradiation with a 4.5 GeV proton beam of 1MW intensity impinging a solid target. The packed-bed target with titanium spheres chosen as the baseline target option is modelised as a continuous media with a reduced density of 3 gr/cm^3 [10].

### 6.2. Target and horn studies.

The packed-bed target is placed inside the upstream part of horn's inner conductor and will be represented in the simulation as a cylinder 78 cm long with radius 1.5 cm.

6.2.1. Induced Activation

The evolution of the induced activation has been estimated as function of cooling time for the target and the horn. The value of the specific activity is obtained as a mean value over the total mass of the considered element.

The activation of the target is non-uniform and present the most active part upstream of the target. The profile of the activation follows the energy deposition inside the target with respect to the beam profile Fig. 22.

After one year of cooling times, the remaining radionucleides contributing to the total activity of the horn qre ^{3}H, ^{7}Be, ^{10}B, ^{14}C, ^{22}Na and ^{26}Al (Fig. 23) but only gamma emitters have a significant impact on the radiological aspect especially in the case of ^{7}Be, ^{22}Na and the long-lived isotopes ^{26}Al.
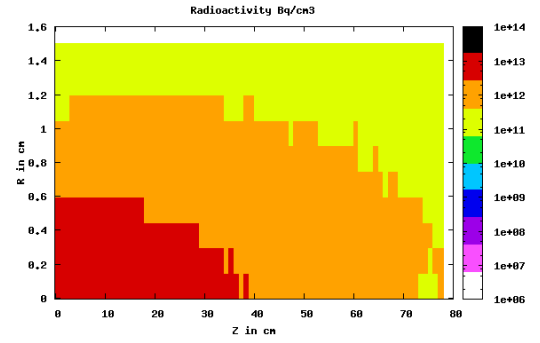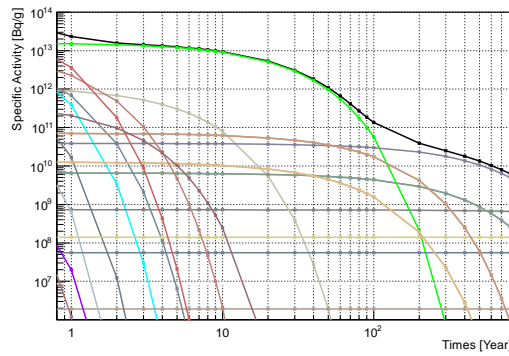
a) Evolution of the specific activity with cooling times.

b) Spatial distribution of activation in the target.

Figure 22: Specific activity of the target.
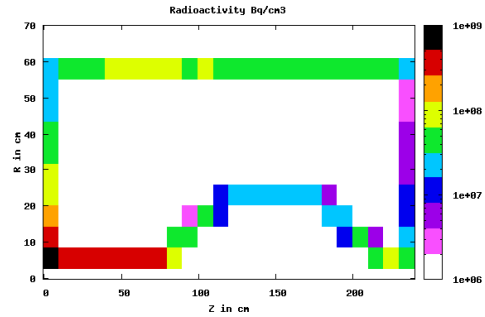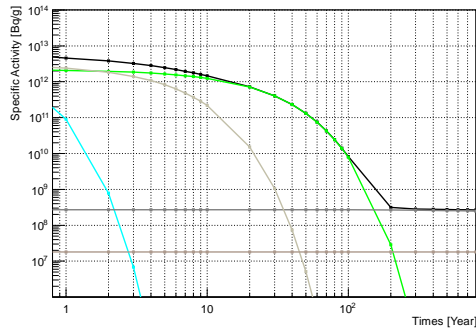
a) Specific Activity with cooling times.

b) Spatial distribution of activation.

Figure 23: Specific activity of the horn.

38

As in the case of the titanium target, the activation in not uniform inside the horn and presents the most active region in the inner conductor as expected (Fig. 23b). Precautions has to be taken in the building of this part of the inner conductor to prevent cracks due to the amount of radiations (water leaks...)

6.2.2. Dose Equivalent Rate

A simplified simulation has been realized to evaluate the contribution to the ambient dose rate around of the target and the horn thanks to the AMB74 option of FLUKA [50]. In this study, a two step method has been used to evaluate the contribution of each of the elements [51]. In this simplified model, all the elements contribute to the dose rate at a non negligeable level the vessel has an importat contribution. The concrete has the lower contribution to the dose rate but the vessel act as a thin shield in the evaluation. After one year of operation, the contribution of the horn is still high to the level of 1 Sv/h which prevent human intervention even by removing the target which is the most active part by two order of magnitude compared to the horn.

6.3. Superbeam Facility

The design of the superbeam facility take advantage of other experiments working with high intensity proton beam such CNGS and T2K experiments.

Secondary charged particles coming out from the pulsed horn will go through the other horns. The total energy deposited on the others horns is a less than 10 % of the pulsed one.

6.3.1. Surrounding iron

The simulated geometry and the power densities of the surrounding iron and concrete of the four-horn area are presented in Table 6 . Results are presented for both neutrino and anti-neutrino beams. A small increase in energy deposition for the anti-neutrino beam is due to positive pions de-focusing: more positive secondary particles are produced due to proton-beam charge. Minimal energy deposition is seen on the concrete after the iron. The iron vessel and the shield will be cooled with water pipes.

6.3.2. Decay tunnel

The decay tunnel area (Fig. 24) consists of the main iron vessel where the particles decay and neutrinos are produced, and the concrete surroundings in order to protect the molasse from activation. At the beginning of the decay tunnel an

horns-targets area length = 7.1 m	target	horn	iron t = 2.2 m x=-4.9 − > 4.9 m	concrete t (above horns) = 1.5 m t (surrounding) = 3.1 m x = -8 − > 8 m
v beam (kW)	85	32	437	0.01
anti-v beam (kW)	85	32	496	0.01

Table 6: Energy deposition in kW for the horns, iron, and concrete around four-horn system for 4 MW proton beam. In this calculation, an outer conductor and upstream plate thickness of 10 mm has been considered for the horn.
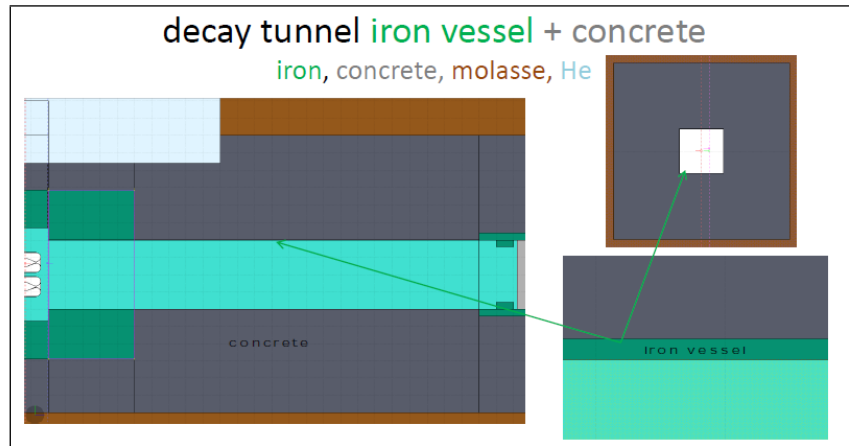

Figure 24: Decay Tunnel layout.

upstream iron-shield is also foreseen to protect the areas above it like the strip-lines. The horn power supply will be built above the start of the decay tunnel.

The energy deposition and the dimensions and thicknesses for the decay-tunnel iron vessel, concrete and upstream iron collimator are shown in Table 7 and Table 8. That geometry is optimized to keep the activation at minimum level in molasse. The decay tunnel vessel will be cooled by water pipes.

area length = 25 m	DT iron vessel H, W = 4 m t = 1.6 cm	DT surrounding concrete t = 6 m
v beam (kW)	390	485
anti-v beam (kW)	392	588

Table 7: Energy deposition in kW for the decay tunnel iron vessel and surrounding concrete.

area length = 25 m	DT iron shield t = 2.9 m x = -4.9 − > 4.9 m	DT iron shield-above decay tunnel t = 2.9
v beam (kW)	610	159
anti-v beam (kW)	775	201

Table 8: Energy deposition in kW for the decay tunnel upstream iron shield .

Preliminary calculation within the WP2 group show that water-cooling is feasible for the decay tunnel vessel.

6.3.3. *Beam dump*

The beam dump area for the SPL Super Beam follows the design of the T2K [52]. It consists of the main graphite block and several shields (25) with the purpose to dump the remaining hadron particles and finally confine the hadronic energy within the experimental layout.

The energy deposition values are shown in Table 9. As seen in the plots the beam dump absorbs all the remaining hadrons so the activation of molasse or any other installation after the beam is prevented. As a result of that, high power dissipation is developed on the dump. On-going studies show the graphite beam dump operation will be feasible by using helium conduction along gaps in graphite. Additional studies show that the induced radioactivity in molasse is kept well under the CERN's limits [53].
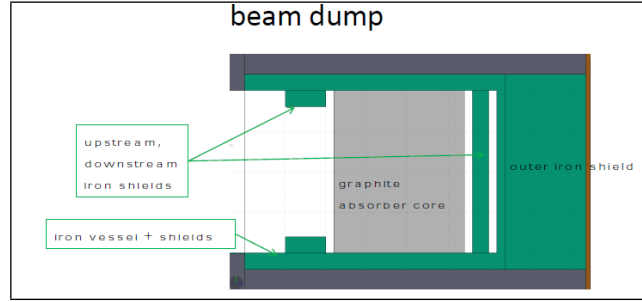
Figure 25: Beam dump layout used in simulation. Graphite beam dump in grey and several iron shields in green.

area length = 6.4 m	graphite L = 3.2 m H, W = 4 m	up-shield	down-shield	outer shield	surrounding concrete t = 6 m
v beam (kW)	778	146	19	1.6	4
anti-v beam (kW)	485	128	12	1	3.6

Table 9: Total energy deposition in kW for the graphite beam dump and various shields..

6.3.4. Summary

With this simulation, we have studied the power dissipation on different elements of the Super Beam. The summary for the neutrino and anti-neutrino beam is presented in Fig. 26. These data are used as input to the finite-elements calculations for the heat dissipation and the design of the cooling methods for the titanium target, the aluminum horn and the graphite beam dump [10].

6.3.5. Shielding investigation

A first approach for the estimation of the shielding is based on a geometry consisting of a simple iron layer surrounded by concrete. The prompt dose rate can be estimated by using an empirical formulae giving the attenuation:

$$H = \frac{H(\theta)}{R^2}.e^{-\frac{t}{\lambda}}$$

with t the total thickness of the material and λ the equivalent length in iron and concrete.

If the design of the structure of the shielding element is kept similar to the T2K, by considering the 2.2m of iron, the concrete thichness should reach 3.7 m
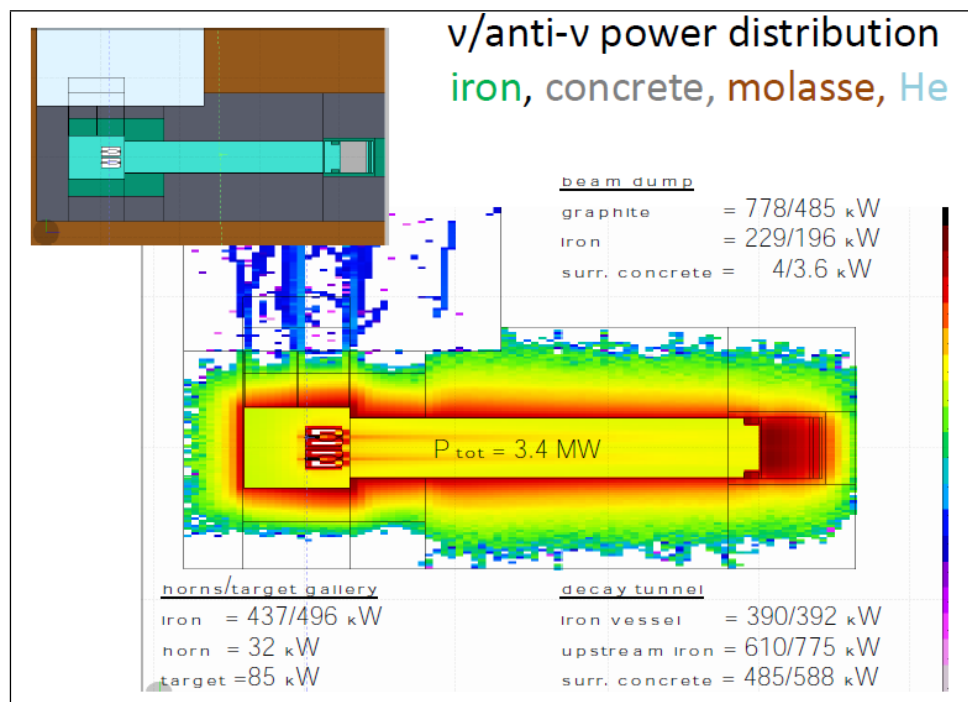
42

Figure 26: Summary of the power densities for the neutrino and anti-neutrino Super Beams.

to decrease the prompt dose rate at a level of $10 \ \mu Sv$.

7. Optimization, fluxes and sensitivity

7.1. Physics performances

This section summarizes the main results appearing in [54].

The neutrino energy spectra are calculated using a probabilistic approach in order to obtain reliable results in a reasonable amount of time using samples of $\sim 10^6$ simulated protons. The probability that the neutrino will reach the far detector is calculated at each particle decay yielding neutrinos with analytic formulas [7, 9, 57, 28]. The probability is then used as a weight factor in the calculation of the neutrino energy spectrum. Neutrinos from hadron interactions in the walls of the decay tunnel or in the beam dump are neglected in this approach.

The distribution of the secondaries at target exit obtained with the FLUKA [55] generator is used as an external input to a GEANT4 [56] simulation derived from a GEANT3 code developed in [7]. The target, the horn with its magnetic field and the decay tunnel are fully simulated within GEANT4. Alternatively GEANT4 can be used to simulate also the interactions of primary protons in the target: this option was used as cross check. In order to cross-check and validate the new GEANT4–based software, a comparison has been done with the fluxes obtained with GEANT3. The fluxes obtained in the two frameworks are in good agreement both in terms of normalization and shape [58]. Further cross-checks included the correct implementation of the decay branching ratios, a comparison with an independent code and a check based on direct scoring of the emitted neutrinos.

The sensitivities for the measurement of the oscillation parameters θ_{13} and δ_{CP} are obtained with the help of GLoBES 3.0.14 [59].

7.2. Target and horn optimization

The approach which was followed in the optimization of the forward–closed horn and the decay tunnel uses the final $\sin^2 2\theta_{13}$ sensitivity. This is a way to maximise the flux at the first oscillation maximum. In this way the final physics performance is used as a guiding principle in the ranking of the configurations under scrutiny. In the evaluation of this quantity a complex set of relevant factors are given as an input: the normalization and shape of each neutrino flavor, the running time in the positive and negative focusing mode, the energy dependence of the cross sections, the backgrounds in the far detector and its response in terms of efficiency and resolution.

We define the δ_{CP}-dependent 99% C.L. sensitivity limit as $\lambda_{99}(\delta_{CP})$. Averaging on δ_{CP} and multiplying by 10^3 we introduce:

$$\lambda = \frac{10^3}{2\pi} \int_0^{2\pi} \lambda_{99}(\delta_{CP})\, d\delta_{CP} \tag{4}$$

This quantity has been used as a practical way of defining with a single number the quality of the focusing system.

The key parameters defining the horn and tunnel geometry are randomly sampled within specified ranges and the correlations with the figure of merit λ studied.

The parameters of the forward–closed horn and of the decay tunnel were sampled with uniform probability distributions imposing the configuration to be geometrically consistent ("iteration-1"). After studying the correlation of these parameters with the figure of merit, a second iteration was performed with a restriction of the phase spaces around the most promising values. The geometrical parameters obtained with this optimization have been reported previously in this article.

7.3. Beam fluxes

The obtained ν_μ, ν_e and charged conjugate (c.c.) neutrino fluxes are shown in Fig. 27 for positive (left) and negative focusing (right) runs. They correspond to $5.6 \cdot 10^{22}$ protons on target (p.o.t.)/year (4 MW $\cdot$ 10^7 s at 4.5 GeV) and are calculated at a reference distance of 100 km over a surface of 100 m^2. The fractions of ν_μ, $\bar{\nu}_\mu$, ν_e and $\bar{\nu}_e$ with respect to the total are (98.0%, 1.6%, 0.42%, 0.015%) and (4.4%, 95.3%, 0.05%, 0.28%) for the positive and negative focusing modes respectively.

focusing	ν_μ	$\bar{\nu}_\mu$	ν_e	$\bar{\nu}_e$
+	$3.9 \cdot 10^{14}$	$6.3 \cdot 10^{12}$	$1.7 \cdot 10^{12}$	$6.0 \cdot 10^{10}$
	98.0%	1.6%	0.42%	0.015%
-	$1.0 \cdot 10^{13}$	$2.2 \cdot 10^{14}$	$1.2 \cdot 10^{11}$	$6.4 \cdot 10^{11}$
	4.4%	95.3%	0.05%	0.28%

Table 10: Integral neutrino flux per year for each flavor at a distance of 100 km over a surface of 100 m^2. The fluxes were obtained with a sample of 10^7 simulated proton-target interactions.

In positive (negative) focusing mode the ν_e ($\bar{\nu}_e$) fluxes are dominated by muon decays: 82% (90%). The c.c. fluxes receive instead a large contribution from kaon three body decays (81% and 75% in positive and negative focusing respectively)
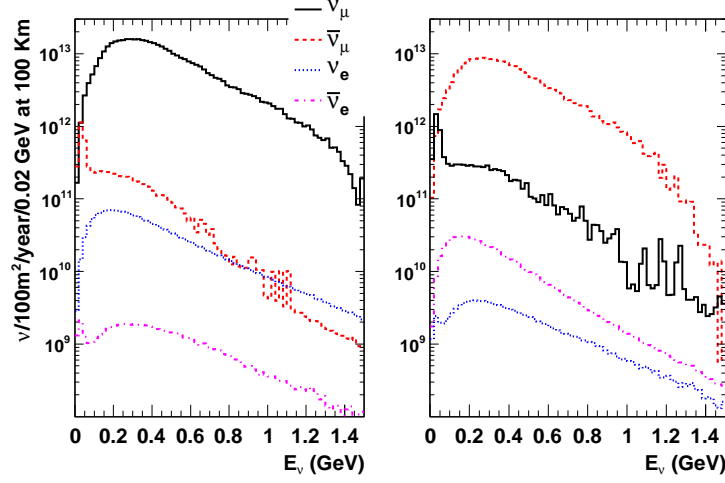
Figure 27: Neutrino fluxes obtained with the optimized horn and decay tunnel in positive (left) and negative (right) focusing mode.

with muon decays from the decay chain of "wronge charge" pions at low energy contributing for the rest. The fluxes are publicly available [60].

The fluxes obtained with the optimized horn have been compared to those obtained with the original double conical horn with currents of 300 and 600 kA associated with a mercury target and published in [9]. The ν_μ and ν_e energy spectra are shifted to higher energies with an increase in statistics particularly around 500 MeV. The ν_μ flux is enhanced also in the proximity of the oscillation maximum at 260 MeV where the ν_e flux is reduced by a similar fraction. The wrong-CP component ($\bar{\nu}_e$, $\bar{\nu}_\mu$) on the other hand is reduced by more than a factor two.

7.4. Physics performances

The CPV discovery potential at the 3 σ level is shown in Fig. 29: discovery is possible in the region above the curves. This means that in that region of the true ($\sin^2 2\theta_{13}$, δ_{CP}) plane a fit done under the CP conserving hypotheses ($\delta_{CP} = 0, \pi$) gives for both choices a $\Delta\chi^2 > 9$. The limit obtained with the previous setup associated with the mercury target is shown by the dash-dotted curve while the new limits are represented as a hatched band. The upper edge of the band (continuous line) refers to the FLUKA model of hadro-production, the lower edge (dotted) to the GEANT4-QGSP model, the one lying (mostly) in the middle (long
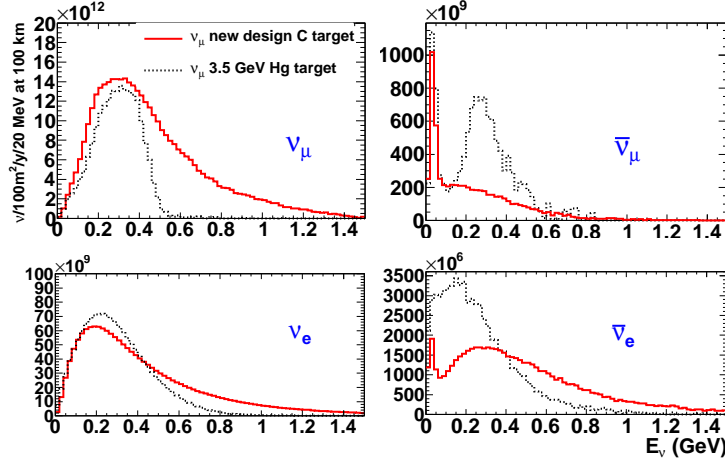
46

Figure 28: Comparison of the neutrino fluxes obtained with the new design (continuous line) and the previous one [9] (dotted line)

dash-dotted) is obtained after reweighting FLUKA with the HARP data. The new limits generally improve those obtained with the previous design both for θ_{13} and CPV discovery.

8. Conclusions

This study is the first that presents a clear and complete conceptual design for a very challenging facility, capable of delivering a low energy neutrino beam with a 4 MW 4.5 GeV/c proton driver. We have presented a novel design for the target, using both a split proton beam to divide the power on each device by a factor four and a pebble bed target. The latter allows the coolant to dissipate in a very efficient way the heat, flowing through the innermost part of the target. The structure of the Ti spheres is such that they will stand the static and dynamic stresses. Preliminary calculations show that this target will be able to stand not only 1 MW per device, as originally required, but probably a higher power. This feature makes it a very attractive solution also for other facilities and in particular it could serve as the target of a neutrino factory.

The focusing device, a magnetic horn, based on a conventional design, has been optimized for our needs on the basis of new approach that allow to study a large parameter space, defined by its geometry, material thickness, current and the decay tunnel characteristics. This optimization has allowed to maintain the ex-
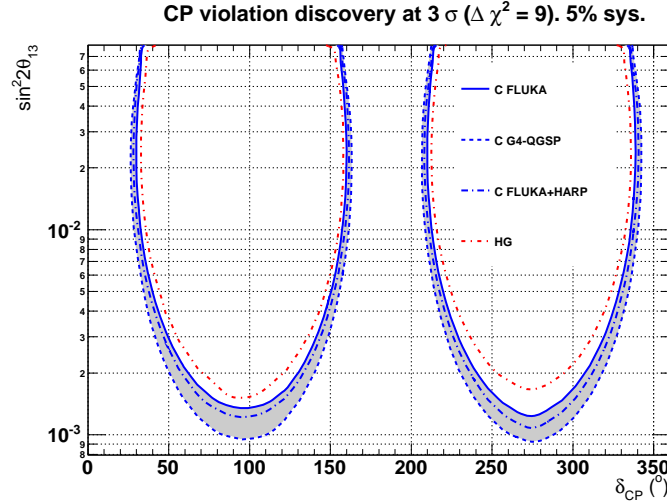
Figure 29: CP violation discovery potential at 3 σ level. See text.

cellent physics performances while offering a realistic design. Preliminary study conclude that the lifetime of each device will be sufficient for a routine operation with high reliability. A difficult but key component is the power supply, subject to an unusual high repetition rate of 50 Hz for a peak current of 300 kA.

We have studied most of the system features, starting from the proton beam exiting from the accumulator up to the beam dump. This has required a diverse array of complementary competences and studies which are only briefly summarized here. Our main conclusion is that this project is feasible by adopting the novel approach that we have introduced and developed here. We have fully studied the shielding and activation issues, to comply with existing radiological regulations, and found that the shileding type and thicknesses, while sizeable, are not excessive neither in terms of engineering nor of cost. In general, while some of the problems that we had in front of us at the start of the project were particularly challenging, we have found no show-stopper and are confident that this project could be built.

Of course, this study, developed within the context of EUROnu, was limited to the engineering and simulations levels. Some of the devices considered here are novel and would require an extensive phase of R/D to assess their performances and validate with a prototype their use in this context.

Acknowledgments

References

[1] C. Bobeth *et al.* EUROnu-WP2-12-xx.

[2] The WP2 reports can be found on www.euronu.org

[3] A. E. Ball, N. Vassilopoulos, A. Blondel and S. S. Gilardoni, "Updated results of the horn study for the Nufact," Nucl. Instrum. Meth. A **472**, 650 (2000), CERN-NUFACT-NOTE-42, CERN-OPEN-2000-339.

[4] S. S. Gilardoni, "Study of particle production and capture for a neutrino factory," CERN-THESIS-2004-046, CERN-NUFACT-NOTE-141, GENEVA-THESE-3536, Jul 2004.

[5] M. Mezzetto, J. Phys. **G29** (2003), 1781-1784,

[6] S. Gilardoni *et al.* J. Phys. G **29**, 1801 (2003).

[7] J.E. Campagne, A. Cazes, Eur. Phys. J. C **45**, 643 (2006).

[8] J.E. Campagne, CERN-NUFACT-NOTE-138, Jul 2004.

[9] J.E. Campagne *et al.*, JHEP **0704**, 003 (2007).

[10] C. Bobeth *et al* 2011 *The target and horn for the SPL-based Super Beam: preliminary design report* (EUROnu-WP2-11-01) http://www.euronu.org

[11] *Conceptual design of the SPL II : A high-power superconducting H- linac at CERN*, M. Baylac et al., CERN-2006-006

[12] *Assessment of the basic parameters of the CERN SPL*, O. Brunner et al. CERN-AB-2008-067 BI/RF

[13] *Feasability Study of Accumulator and Compressor for the 6-bunches SPL based Proton Driver*, M. Aiba, CERN-AB-2008-060-B1, September 2008, CERN

[14] R. Garoby, CERN, Private communication, 02-05-12

[15] *The proton driver for the neutrino Super Beam: status and issues*, C. Bobeth et al., EUROnu WP2 Note 09-11, http://www.euronu.org/

[16] *Study of a horn with integrated target for a Neutrino Factory* , J. M. Maugain, S. Rangod, F. Voelker, CERN-

[17] *Beam stability in the SPL-Proton Driver accumulator for a Neutrino Factory at CERN*, E. Benedetto, CERN-BE-2009-037, CERN-NUFACT-Note-156, Proc. NUFACT'09: 11th International Workshop on Neutrino Factories, Superbeams and Beta Beams, July 20-25, 2009, Chicago

[18] E. Benedetto, CERN, private communication, Feb.2012

[19] *SPL Transfer Line*, P.A. Posocco, sLHC Project Note 0038, 2012-04-17, CERN

[20] *Solid target cooling for high power neutrino SPL-Super Beam*, B. Lepers et al., EUROnu WP2 Note 10-03 (internal note), IPHC/CNRS, 2010

[21] PSI Graphic Transport Framework by U. Rohrer based on a CERN-SLAC-FERMILAB version by K.L. Brown et al

[22] A. Lombardi, CERN, private communication, 27-06-12

[23] P. Poussot, IPHC, Strasbourg, private communication, 16-05-2012

[24] 'The T2K Experiment', K. Abe et al. (T2K Collaboration), (2011), accepted in Nucl. Instrum. Methods, doi: 10.1016/j.nima.2011.06.067,arXiv:1106.1238 [physics.ins-det]

[25] Ergun, S., "Fluid Flow Through Packed Columns", Chem. Eng. Progress, 48, 89- 94 (1952).

[26] E.Achenbach "Heat Transfer and Pressure Drop of Pebble Beds up to High Reynolds Number" 7th International Heat Transfer Conference 1982 Munich Germany Shelfmark: 4276:093000

[27] Pugnat and Sievers "A helium gas cooled stationary granular target" CERN NUFACT Note 121, 2003 J. Phys. G: Nucl. Part. Phys. 29 1797

[28] A. Cazes, "Study of the CNGS beam and muon identification with the OPERA experiment. Optimization of the SPL-Frejus project beam line," LAL-04-118, Ph.D. Thesis, Dec 2004.

[29] A. Longhin, "A new design for the CERN Frejus neutrino Super Beam" EUROnu WP2-10-04.

[30] C. Bobeth and A. Longhin "Optimisation of hadron focusing for the SPL-Frejus Super Beam" EUROnu WP2-10-02, 2010.

[31] S. van der Meer, "A directive device for charged particles and its use in an enhanced neutrino beam," CERN-61-07.

[32] G. Yahr "Fatigue design curves for 6061-T' Aluminium" Engineering Technology Division Oak Ridge National Laboratory

[33] B. Lepers, EUROnu WP2 note 6, 2011 "Study a water jet cooling system for an electromagnetic horn"

[34] Manuel Lorenzo Sentis, Alfredo Ferrari, Stephane Rangod, "Analytical Estimation of the Water Thickness around the Inner Conductor of the CNGS Magnetic Horn", CNGS internal report 2006

[35] Private communication, K. Anderson, Fermilab/Accelerator Division, 2006

[36] H. Hirshfeld et al., "High heat flux cooling of accelerator targets with microchannels", NIM A 562, 2006

[37] All "Technical design report for the MiniBOONE neutrino beam "

[38] Yahr G 1993 *Proc. Conf. on Codes and Standards in a Global Environment (Colorado)* ed J Staffiera (American Society of Mechanical Engineers) p 43

[39] Yahr G 1993 Fatigue design curves for 6061-T6 Aluminum *Codes and Standards in a Global Enviroment* PVP-Vol. **83** 43-9

[40] P. Cupial, "MiniBoone like horn, dynamic response to magnetic and thermal pulses", EUROnu annual meeting, RAL January 2011

[41] M.S Kozien,"Horn fatigue life estimation under magnetic forces", EUROnu-WP2 meeting, November 2011

[42] J. Campagne, S. Wallon and B. Kapusta "Influence des neutrons thermiques et rapides sur les alliages d'aluminium de la serie 6000"

[43] N. Simos, "Superbeam Horn-Target Integration", EUROnu-IDS Target Meeting, December 2008

[44] N. Simos, "Horn-Target Material Studies at BNL, towards multi-MW Beam", LBNE Science Collaboration, FNAL meeting, July 2009

[45] B. Skocze, A. Ustrzycka,"Target-horn integration and degradation of material properties due to radiation", EUROnu-WP2 meeting, March 2012

[46] A. Ustrzycka, B. Skocze,"Degradation of material properties and lifetime estimation of horn under irradiation and mechanical loads", EUROnu-WP2 meeting, May 2012

[47] P. Poussot *et al* July 2012 *Study of 4 horns 350kA peak current, 100 μs large 50Hz electric power supply unit (PSU) with coupled direct devices.* EUROnu WP2 Note 15 http://www.euronu.org.

[48] "FLUKA: a multi-particle transport code" A. Ferrari, P.R. Sala, A. Fasso', and J. Ranft, CERN-2005-10 (2005), INFN-TC-05-11, SLAC-R-773

[49] V.Vlachoudis "FLAIR: A Powerful But User Friendly Graphical Interface For FLUKA" Proc. Int. Conf. on Mathematics, Computational Methods & Reactor Physics (M&C 2009), Saratoga Springs, New York, 2009

[50] M. Pelliccioni, "Overview of fluence-to-effective dose and fluence-to-ambient dose equivalent conversion coefficients for high energy radiation calculated using the FLUKA code" Rad. Prot. Dosim. 88, 279-297 (2000)

[51] Stefan Roesler, private communication

[52] Several presentations on T2K experiment in Neutrino Beam Instrumentation Workshops as NIB 2005 http://www.hep.utexas.edu/nbi2005/

[53] S. Agosteo *et al* 2003 *Induced Radioacticity in a 4 MW Target and its Surroundings* (CERN-TIS-2003-003-RP-CF)

[54] A. Longhin, EPJC 2011, 71, 9, 1745.

[55] G. Battistoni *et al.*, AIP Conf. Proc. **896**, 31 (2007).

[56] N IM A **506** (2003) 250-303.

[57] A. Blondel *et al.*, CERN-NUFACT-NOTE-53, CERN-OPEN-2000-343, Nov 2000. CERN-NUFACT-NOTE-78, Sep 2001.

[58] A. Longhin, AIP Conf. Proc. 1222 (2010) 339-343.

[59] P. Huber *et al.*, Comput. Phys. Commun. **177**, 432 (2007).

[60] `http://irfu.cea.fr/en/Phocea/Pisp/index.php?id=54`